BMC Anesthesiology

RESEARCH

Open Access

Trichloroethanol, an active metabolite of chloral hydrate, modulates tetrodotoxin-resistant Na^+ channels in rat nociceptive neurons

Gimin Kim[1], Hyunjung Kim[1] and Il-Sung Jang[2,3*]

Abstract

Background Chloral hydrate is a sedative-hypnotic drug widely used for relieving fear and anxiety in pediatric patients. However, mechanisms underlying the chloral hydrate-mediated analgesic action remain unexplored. Therefore, we investigated the effect of 2′,2′,2′-trichloroethanol (TCE), the active metabolite of chloral hydrate, on tetrodotoxin-resistant (TTX-R) Na^+ channels expressed in nociceptive sensory neurons.

Methods The TTX-R Na^+ current (I_{Na}) was recorded from acutely isolated rat trigeminal ganglion neurons using the whole-cell patch-clamp technique.

Results Trichloroethanol decreased the peak amplitude of transient TTX-R I_{Na} in a concentration-dependent manner and potently inhibited persistent components of transient TTX-R I_{Na} and slow voltage-ramp-induced I_{Na} at clinically relevant concentrations. Trichloroethanol exerted multiple effects on various properties of TTX-R Na^+ channels; it (1) induced a hyperpolarizing shift on the steady-state fast inactivation relationship, (2) increased use-dependent inhibition, (3) accelerated the onset of inactivation, and (4) retarded the recovery of inactivated TTX-R Na^+ channels. Under current-clamp conditions, TCE increased the threshold for the generation of action potentials, as well as decreased the number of action potentials elicited by depolarizing current stimuli.

Conclusions Our findings suggest that chloral hydrate, through its active metabolite TCE, inhibits TTX-R I_{Na} and modulates various properties of these channels, resulting in the decreased excitability of nociceptive neurons. These pharmacological characteristics provide novel insights into the analgesic efficacy exerted by chloral hydrate.

Keywords Chloral hydrate, Trichloroethanol, Analgesia, TTX-R Na^+ channels, Nociceptive neurons, Patch clamp

*Correspondence:
Il-Sung Jang
jis7619@knu.ac.kr
Full list of author information is available at the end of the article

Background

Nociceptive signals generated at peripheral tissues are transmitted to the central nervous system through the generation and conduction of action potentials. Thus, various voltage-gated ion channels, such as voltage-gated Na^+ and K^+ channels, expressed in sensory neurons play pivotal roles in nociceptive transmission. Among the nine types of voltage-gated Na^+ channels, tetrodotoxin-sensitive (TTX-S) $Na_V1.7$ and TTX-resistant (TTX-R) $Na_V1.8$ and $Na_V1.9$ are specifically expressed in nociceptive sensory neurons within the dorsal root ganglia (DRG) and trigeminal ganglia (TG) [1]. In particular, $Na_V1.8$ plays a pivotal role in the generation and conduction of action potentials in response to sustained nociceptive signals, as this channel remains activated even at relatively depolarized membrane potentials [2, 3]. $Na_V1.8$ has also been implicated in the development and maintenance of inflammatory hyperalgesia [4]. We reported that the TTX-R Na^+ channels ($Na_V1.8$)-mediated persistent Na^+ current (I_{NaP}), which is a non-inactivating current during sustained depolarizing stimuli, contributes to the excitability of nociceptive neurons, and the density of TTX-R I_{NaP} is increased by inflammatory mediators [5]. These findings suggest that TTX-R Na^+ channels and TTX-R I_{NaP} mediated by the $Na_V1.8$ subtype are potential pharmacological targets for relieving inflammatory pain [1].

Children are mentally, physically, and emotionally immature, and those visiting the dentist for the first time have heightened fear and anxiety about dental treatment. Although various psychological and physical methods, such as voice control and mouth covering, can be used to control behavioral states, such methods are not always successful. Therefore, behavioral control using sedative and anesthetic agents, such as chloral hydrate, midazolam, and nitrous oxide, is recommended for the dental treatment of pediatric patients [6].

Chloral hydrate, a first-generation sedative-hypnotic drug, is used for sedation and for relieving fear and anxiety in pediatric patients undergoing medical procedures [7, 8], such as dental treatment [6, 7, 9]; however, its use in humans or animals has been declining [10–12]. Chloral hydrate is readily absorbed after oral administration but is undetectable 10 min after intake because of its rapid metabolization by aldehyde dehydrogenase in hepatocytes and erythrocytes [8, 11–13]. Owing to its rapid conversion after oral administration, most pharmacological properties of chloral hydrate have been determined using its active metabolite 2′,2′,2′-trichloroethanol (TCE) [14]. Although the mechanisms underlying the sedative and anesthetic action of chloral hydrate or TCE remain poorly understood, TCE is known to act on $GABA_A$ receptors to potentiate Cl^- conductance in the central nervous system, similar to benzodiazepines [15]. Notably, TCE potentiates native [15] and recombinant [16] $GABA_A$ receptors expressed in mouse hippocampal neurons and HEK 293 cells, respectively. TCE also potentiates recombinant glycine and 5-HT_3 receptors expressed in *Xenopus* oocytes [17, 18]. In addition, TCE reportedly inhibits excitatory glutamate receptors, such as AMPA and NMDA receptors, in central neurons [19, 20]. Such direct modulation of inhibitory or excitatory receptors might be responsible for the sedative and hypnotic actions mediated by chloral hydrate. While it is not directly related to the anesthetic efficacy, TCE also inhibits mitochondrial ATP-sensitive K^+ channels in rat cardiac myocytes [21].

In addition to its anesthetic action, chloral hydrate reportedly exhibits analgesic effects [7, 22]. Such analgesic effects might result from the modulation of nociceptive transmission; however, limited information is available regarding the mechanisms underlying the analgesic action of chloral hydrate. Therefore, in this study, we examined the effect of TCE on TTX-R Na^+ channels in acutely isolated nociceptive neurons. To our knowledge, this is the first study describing the pharmacological role of TCE in peripheral analgesic efficacy.

Materials and methods

Preparation

All experiments in this study complied with the guiding principles for the care and use of animals and were approved by the Council of Kyungpook National University (KNU-2019-0053). Every effort was made to minimize the number of animals used and their suffering.

Sprague Dawley rats (postnatal age: 3–4 weeks; both sexes; Samtako, Osan, Korea) were decapitated under ketamine anesthesia (50 mg/kg, intraperitoneal). Their TGs (V_3 part) were dissected and treated with a standard external solution (150 mM NaCl, 3 mM KCl, 2 mM $CaCl_2$, 1 mM $MgCl_2$, 10 mM glucose, and 10 mM HEPES, [pH 7.4 with Tris-base]) containing 0.3% collagenase and 0.3% trypsin at 37 °C for 40–50 min. Subsequently, TG neurons were mechanically dissociated by trituration using fire-polished Pasteur pipettes in culture dishes (CELLSTAR® TC, Greiner bio-one, Chonburi, Thailand). Isolated TG neurons were used for electrophysiological recordings 2–6 h after preparation.

Electrical measurements

Electrical measurement data were collected using conventional whole-cell patch recordings and a standard patch-clamp amplifier (Multiclamp 900B; Molecular Devices, Union City, CA, USA). Neurons were voltage clamped at a holding potential (V_H) of −80 mV. Patch pipettes were

prepared from borosilicate capillary glass (G-1.5; Narishige, Tokyo, Japan) using a pipette puller (P-97; Sutter Instrument Co., Novato, CA, USA). The resistance of recording pipettes filled with an internal solution (135 mM CsF, 10 mM CsCl, 2 mM EGTA, 2 mM ATP-Na_2, and 10 mM HEPES [pH 7.2 with Tris-base]) was 0.7–1.0 MΩ. Membrane potentials were corrected for the liquid junction potential, and the pipette capacitance and series resistance (40–70%) were compensated for. Neurons were viewed under phase contrast on an inverted microscope (TE2000; Nikon, Tokyo, Japan). Membrane currents were filtered at 2–5 kHz, digitized at 10–20 kHz, and stored on a computer equipped with pCLAMP 10.7 (Molecular Devices). The bath solution was composed of: 130 mM NaCl, 20 mM tetraethylammonium-Cl, 2 mM $CaCl_2$, 1 mM $MgCl_2$, 10 mM HEPES, 10 mM glucose, 0.0003 mM TTX, and 0.01 mM $CdCl_2$ (pH 7.4 with Tris-base), except where indicated. To record TTX-R I_{Na}, capacitative and leakage currents were subtracted using the P/4 subtraction protocol (pCLAMP 10.7). The internal solution used in the current-clamp experiments for recording voltage responses was composed of 135 mM KF, 10 mM KCl, 2 mM EGTA, 2 mM ATP-Na_2, and 10 mM HEPES (pH 7.2 with Tris-base), whereas the external solution was composed of 150 mM NaCl, 3 mM KCl, 2 mM $CaCl_2$, 1 mM $MgCl_2$, 10 mM glucose, 10 mM HEPES, and 0.0003 mM TTX (pH 7.4 with Tris-base).

Data analysis

The peak amplitude, time to peak, and decay time constant of the transient TTX-R I_{Na} were determined using pCLAMP 10.7. In a subset of measurements, the amplitude of TTX-R I_{Na} was transformed into conductance (G) using the following equation:

$$G = I/(V - E_{Na})$$

The voltage-activation and voltage-inactivation relationships of TTX-R Na^+ channels were respectively fitted to the following Boltzmann equations:

$$G/G_{max} = 1/\left(1 + \exp\left[\left\{V_{50,activation} - V\right\}/k\right]\right) \text{ and } I/I_{max} = 1 - 1/\left(1 + \exp\left[\left\{V_{50,inactivation} - V\right\}/k\right]\right),$$

where G_{max} is the maximum conductance, I_{max} is the maximum current amplitude, $V_{50,\ activation}$ is the half-maximum voltage for activation, $V_{50,\ inactivation}$ is the half-maximum voltage for fast inactivation, and k is the slope factor. Kinetic data for the onset of inactivation and recovery from inactivation were fitted to the following equations, respectively:

$$I(t) = A_0 + A_{fast} \times \left(\exp\left[-t/\tau_{fast}\right]\right) + A_{slow} \times \left(\exp\left[-t/\tau_{slow}\right]\right) \text{ and}$$
$$I(t) = A_0 + A_{fast} \times \left(1 - \exp\left[-t/\tau_{fast}\right]\right) + A_{intermediate} \times \left(1 - \exp\left[-t/\tau_{intermediate}\right]\right) + A_{slow} \times \left(1 - \exp\left[-t/\tau_{slow}\right]\right)$$

In these equations, $I(t)$ is the amplitude of TTX-R I_{Na} at time t, whereas A_{fast}, $A_{intermediate}$, and A_{slow} are the amplitude fractions of τ_{fast}, $\tau_{intermediate}$, and τ_{slow}, respectively. The weighted decay time constant (τ_{WD}) for the single transient TTX-R I_{Na} or weighted time constant ($\tau_{weighted}$) for the onset of inactivation was calculated using the following equation:

$$\tau_{WD} \text{ or } \tau_{weighted} = \left(\left[\tau_{fast} \times A_{fast}\right] + \left[\tau_{slow} \times A_{slow}\right]\right)/\left(A_{fast} + A_{slow}\right)$$

The $\tau_{weighted}$ for the recovery from inactivation was calculated using the following equation:

$$\tau_{weighted} = \left(\left[\tau_{fast} \times A_{fast}\right] + \left[\tau_{intermediate} \times A_{intermediate}\right] + \left[\tau_{slow} \times A_{slow}\right]\right)/\left(A_{fast} + A_{intermediate} + A_{slow}\right)$$

Numerical values are provided as the mean ± standard error of the mean (SEM) following normalization to the control value. Significant differences in the mean amplitude were tested with Student's paired two-tailed t-test using absolute rather than normalized values. $P < 0.05$ was considered statistically significant.

Drugs

The drugs used in this study were collagenase (type I), trypsin (type I), tetrodotoxin (TTX), Na-ATP, $CdCl_2$, and 2′,2′,2′-trichloroethanol (TCE) (all from Sigma, USA) and ketamine (Yuhan Co., Seoul, Korea). The extracellular solution containing drugs was applied to patched neurons using the "Y–tube system" for rapid solution exchange [23] at a perfusion rate of 0.5–0.6 mL/min.

Results

Effects of TCE on transient TTX-R Na^+ currents

We first examined the effect of TCE, an active metabolite of chloral hydrate (Fig. 1A), on transient TTX-R I_{Na} in nociceptive neurons using a whole-cell patch-clamp technique. Small-sized DRG neurons (< 30 μm in diameter; 25.0 ± 4.7 pF; $n = 65$ neurons) were held at a V_H of

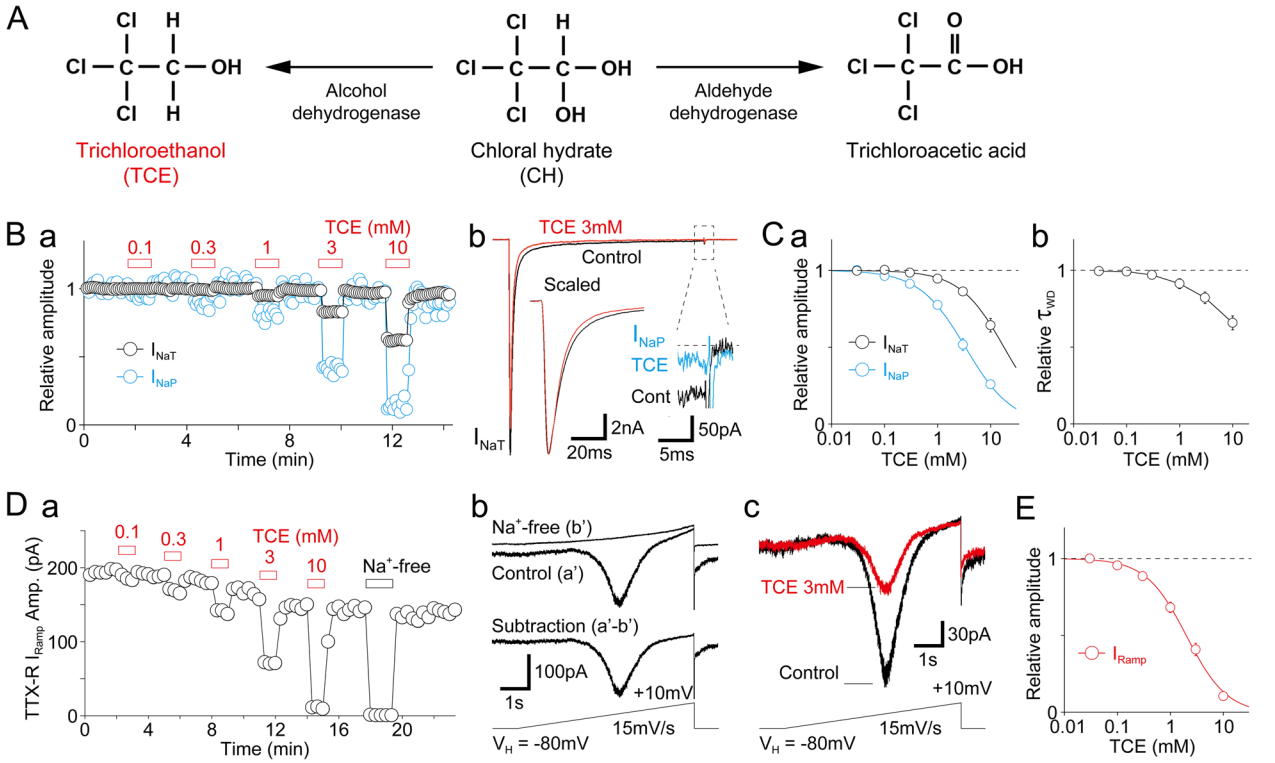

Fig. 1 Effect of TCE on TTX-R I_{Na}. **(A)** A brief illustration showing chloral hydrate (CH) metabolism after absorption. CH is rapidly converted into trichloroethanol (TCE) and trichloroacetic acid by alcohol dehydrogenase and aldehyde dehydrogenase, respectively. TCE is conjugated with glucuronic acid and excreted through the kidneys. **(B) a**, Typical time courses of TTX-R I_{Na} amplitude before and during TCE application to small-sized TG neurons. TTX-R I_{Na} was elicited by electrical stimulation from a V_H of − 80 mV to − 10 mV (100 ms duration) at 5 s intervals. The amplitudes of transient (black circles; I_{NaT}) and persistent (cyan circles; I_{NaP}) TTX-R I_{Na} were normalized to the first amplitude. **b**, Typical traces of TTX-R I_{Na} in the absence and presence of 3 mM TCE. Both I_{NaT} (scaled) and I_{NaP} are presented in expanded time and amplitude scales, respectively (insets). **(C) a**, The concentration-inhibition relationship of TCE for transient (black circles; I_{NaT}) and persistent (cyan circles; I_{NaP}) TTX-R I_{Na}. Continuous lines represent the best fit using the least squares method. Each point represents the mean and SEM from 6–9 experiments. **b**, The concentration-inhibition relationship of TCE for the weighted decay time constant (τ_{WD}) of TTX-R I_{Na}. Each point represents the mean and SEM from seven experiments. **(D) a**, A typical time course of slow voltage ramp-induced current (TTX-R I_{Ramp}) amplitude before and during TCE application to small-sized TG neurons. The TTX-R I_{Ramp} was elicited by slow voltage ramp stimulation from a V_H of − 80 mV to + 10 mV (15 mV/s, every 20 s). **b**, Typical traces of TTX-R I_{Ramp} in the presence (a') and absence (b') of extracellular Na^+. Subtraction (a'–b') of two traces yields TTX-R I_{Ramp} without the capacitative current. **c**, Typical traces of TTX-R I_{Ramp} in the absence and presence of 3 mM TCE. **(E)** The concentration-inhibition relationship of TCE for TTX-R I_{Ramp}. The continuous line represents the best fit using the least squares method. Each point represents the mean and SEM from seven experiments

− 80 mV, and brief depolarizing step pulses (up to − 10 mV, 100-ms duration) were applied to elicit the TTX-R I_{Na}. Under these conditions, the recorded TTX-R I_{Na} was stable, and TCE inhibited the peak amplitude of the transient component of TTX-R I_{Na} (I_{NaT}) in a dose-dependent manner with an IC_{50} value of 18.4 ± 1.1 mM ($n = 7$). In contrast, at a 3 mM concentration, it decreased the amplitude of TTX-R I_{NaT} to 86.3 ± 1.6% of that in the control ($n = 7$, $p < 0.01$; Fig. 1B, Ca). However, TCE more potently inhibited the noninactivating persistent component of transient TTX-R I_{Na} (I_{NaP}) in a dose-dependent manner with an IC_{50} value of 3.3 ± 0.4 mM ($n = 7$). In contrast, at a 3 mM concentration it decreased the amplitude of TTX-R I_{NaP} to 51.7 ± 3.9% of that in the control ($n = 7$, $p < 0.01$; Fig. 1B, Ca). In addition, TCE accelerated the decay phase of a single TTX-R I_{Na} in a dose-dependent manner (Fig. 1Cb). Notably, I_{NaP} can be elicited by slow voltage ramp stimuli [24, 25]. Therefore, we further examined the effect of TCE on the slow voltage ramp-induced current (I_{Ramp}). We determined that TCE potently inhibited the TTX-R I_{Ramp} in a concentration-dependent manner with an IC_{50} value of 2.0 ± 0.2 mM ($n = 7$), whereas at a 3 mM concentration, it reduced the TTX-R I_{Ramp} amplitude to 40.8 ± 4.0% of that in the control ($n = 7$; $p < 0.01$; Fig. 1D, E).

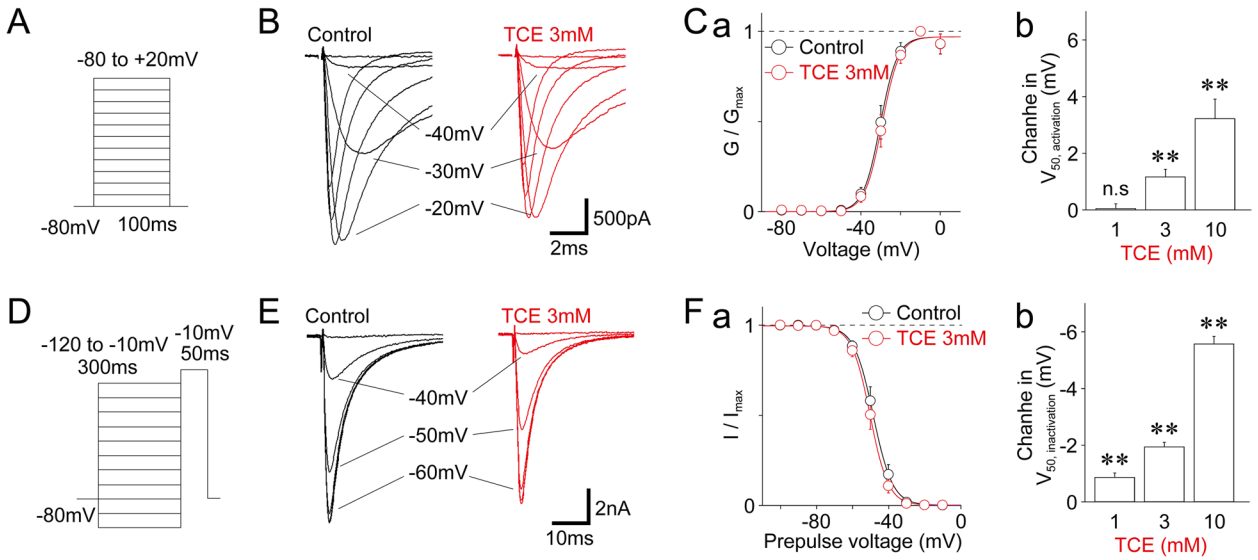

Fig. 2 Effect of TCE on the voltage-dependence of TTX-R Na^+ channels. **(A)** A schematic illustration of voltage step pulses to examine the voltage-activation relationship of TTX-R Na^+ channels. The TTX-R I_{Na} was induced by 50 ms depolarization pulses from − 80 to + 20 mV in 10 mV increments at a V_H of − 80 mV. **(B)** Typical traces of TTX-R I_{Na} elicited by voltage step pulses in the absence (left) and presence (right) of 3 mM TCE. **(C) a**, The conductance-voltage relationship of TTX-R Na^+ channels in the absence (black circles) and presence (red circles) of 3 mM TCE. Continuous lines represent the best fit of the Boltzmann function. Each point represents the mean and SEM from seven experiments. **b**, TCE-induced changes in the midpoint voltage for the activation ($V_{50,\ activation}$) of TTX-R Na^+ channels. Each column represents the mean and SEM from seven experiments for 1, 3, and 10 mM TCE. **; $p < 0.01$, n.s; not significant. **(D)** A schematic illustration of voltage step pulses to examine the voltage-steady state fast inactivation relationship of TTX-R Na^+ channels. The TTX-R I_{Na} was induced by 50 ms depolarization pulses to − 10 mV after 300 ms prepulse from − 120 to − 20 mV in 10 mV increments. **(E)** Typical traces of TTX-R I_{Na} elicited by voltage step pulses in the absence (left) and presence (right) of 3 mM TCE. **(F) a**, The voltage-inactivation relationship of TTX-R Na^+ channels in the absence (black circles) and presence (red circles) of 3 mM TCE. Continuous lines represent the best fit of the Boltzmann function. Each point represents the mean and SEM from seven experiments. **b**, TCE-induced changes in the midpoint voltage for the inactivation ($V_{50,\ inactivation}$) of TTX-R Na^+ channels. Each column represents the mean and SEM from seven experiments for 1, 3, and 10 mM TCE. **; $p < 0.01$

Effects of TCE on the voltage-dependence of TTX-R Na^+ channels

We then examined the effect of TCE on the voltage-activation relationship of TTX-R Na^+ channels using depolarizing test pulses (100-ms duration, up to + 20 mV in 10-mV increments; Fig. 2A). Subsequently, TTX-R I_{Na} was converted to conductance, and the normalized conductance values were fitted to the Boltzmann function. TCE shifted the midpoint voltage for activation ($V_{50,\ activation}$) toward a hyperpolarizing range in a dose-dependent manner. In contrast, at a 3 mM concentration, it changed the $V_{50,\ activation}$ values by 1.2 ± 0.3 mV (-29.8 ± 4.4 mV for the control and -28.6 ± 4.2 mV for TCE treatment; $n = 7$; $p < 0.01$; Fig. 2B, C). Notably, these TCE-induced changes in $V_{50,\ activation}$ values were dose-dependent (Fig. 2Cb). We also examined the effect of TCE on the steady-state voltage-inactivation relationship of TTX-R Na^+ channels using depolarization test pulses (100-ms duration, up to − 10 mV after 300-ms prepulse from − 120 to − 10 mV in 10 mV increments; Fig. 2D). When the normalized TTX-R I_{Na} was fitted to the Boltzmann function, TCE shifted the midpoint voltage for inactivation ($V_{50,\ inactivation}$) toward a hyperpolarizing range in a dose-dependent manner. In contrast, at a 3 mM concentration, it changed the $V_{50,\ inactivation}$ values by -1.9 ± 0.2 mV (-48.3 ± 1.7 mV for the control and -50.2 ± 1.6 mV for TCE treatment; $n = 7$; $p < 0.01$; Fig. 2E, F). These TCE-induced changes in $V_{50,\ inactivation}$ values were dose-dependent (Fig. 2Fb).

Effects of TCE on the use-dependent inhibition of TTX-R Na^+ channels

Next, we examined the effect of TCE on the use-dependence of TTX-R Na^+ channels using a 20 s series of 40 (2 Hz), 100 (5 Hz), and 200 (10 Hz) depolarizing test pulses (10-ms duration, up to − 10 mV; Fig. 3A). Figure 3B depicts typical TTX-R I_{Na} elicited by 200 (10 Hz) depolarizing test pulses in the absence and presence of 3 mM TCE. Figure 3 C displays typical time courses of TTX-R I_{Na} elicited by 40 (2 Hz), 100 (5 Hz), and 200 (10 Hz) depolarizing test pulses in the absence and presence of 3 mM TCE. When the amplitude ratio of the 40th, 100th, and 200th TTX-R I_{Na} (P_{40}, P_{100}, and P_{200}, respectively) and the first TTX-R I_{Na} (P_1) was analyzed, TCE

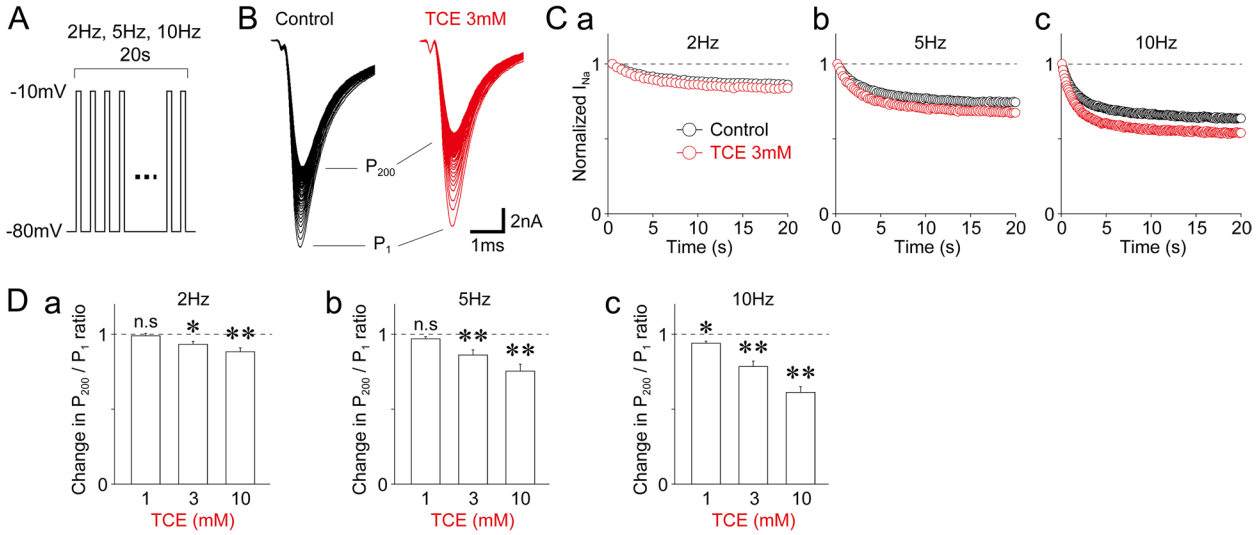

Fig. 3 Effect of TCE on the use-dependent inactivation of TTX-R Na^+ channels. **(A)** A schematic illustration of voltage step pulses to examine the use-dependent inhibition of TTX-R Na^+ channels. The TTX-R I_{Na} was induced by 40, 100, and 200 successive voltage step pulses (− 80 mV to − 10 mV, 10 ms duration, 2 Hz, 5 Hz, and 10 Hz, respectively). **(B)** Typical traces of TTX-R I_{Na} elicited by 200 successive voltage step pulses (10 Hz) in the absence (left) and presence (right) of 3 mM TCE. **(C)** Time courses of the amplitude of TTX-R I_{Na} during trains of 40 (2 Hz, **a**), 100 (5 Hz, **b**), and 200 pulses (10 Hz, **c**) in the absence (black circles) and presence (red circles) of 3 mM TCE. Each point represents the mean and SEM from eight experiments. **(D)** TCE-induced changes in the P_{40}/P_1 (2 Hz, **a**), P_{100}/P_1 (5 Hz, **b**), and P_{200}/P_1 (10 Hz, **c**) ratios of TTX-R I_{Na}. The ratios were normalized to the respective control (dotted lines). Each column represents the mean and SEM from eight experiments for 1, 3, and 10 mM TCE. *; $p < 0.05$, **; $p < 0.01$, n.s; not significant

decreased the P_{40}/P_1, P_{100}/P_1, and P_{200}/P_1 ratios in a dose-dependent manner (Fig. 3D). In contrast, at a 3 mM concentration, it decreased the P_{200}/P_1 ratio to 78.5 ± 3.6% of that in the control ($n = 8$, $p < 0.01$; Fig. 3Dc).

Effects of TCE on inactivation and recovery kinetics of TTX-R Na^+ channels

We examined the effect of TCE on the onset of inactivation of TTX-R Na^+ channels using a two-pulse protocol (first conditioning pulse (P_1): 2–5000-ms duration (up to − 10 mV); second test pulse (P_2): 100-ms duration (up to − 10 mV) with a 20-ms interpulse interval; Fig. 4A). Figure 4B depicts typical TTX-R I_{Na} elicited by a two-pulse protocol in the absence and presence of 3 mM TCE. We analyzed the amplitude ratio of 2 TTX-R I_{Na} (P_2/P_1) to examine the extent of time-dependent inactivation of TTX-R Na^+ channels. We then calculated the P_2/P_1 ratio in the absence and presence of TCE and fitted it to a double exponential function (Fig. 4C). We regarded the two resultant time constants, that is, fast (τ_{fast}) and slow (τ_{slow}), and their amplitude fractions, that is, fast (A_{fast}) and slow (A_{slow}), as the kinetic parameters of the onset of inactivation. As shown in Fig. 4D, TCE at a 3 mM concentration decreased the τ_{fast} (69.3 ± 6.1% of that in the control, 140.3 ± 10.1 ms for the control, and 93.9 ± 4.4 ms for 3 mM TCE treatment; $n = 7$, $p < 0.05$); however, this did not affect the τ_{slow}, A_{fast}, and A_{slow} values. Furthermore, TCE decreased the $\tau_{weighted}$ in a concentration-dependent manner. In contrast, at a 3 mM concentration, it decreased the $\tau_{weighted}$ (81.2 ± 3.6% of that in the control, 796.8 ± 75.4 ms for the control, and 647.6 ± 70.0 ms for 3 mM TCE treatment; $n = 7$, $p < 0.01$; Fig. 4E).

We further examined the effect of TCE on the recovery from the inactivation of TTX-R Na^+ channels using a two-pulse protocol (first conditioning pulse (P_1): 500-ms duration (up to − 10 mV); second test pulse (P_2): 100-ms duration (up to − 10 mV) with recovery times at − 80 mV varying from 1 to 5000 ms; Fig. 5A). Figure 5B displays typical TTX-R I_{Na} elicited by a two-pulse protocol in the absence and presence of 3 mM TCE. We analyzed the amplitude ratio of two TTX-R I_{Na} (P_2/P_1) to examine the extent of time-dependent recovery of TTX-R Na^+ channels. We then calculated the P_2/P_1 ratio in the absence and presence of TCE and fitted it to a triple exponential function (Fig. 5C). We thus regarded the three resultant time constants, that is, fast (τ_{fast}), intermediate ($\tau_{intermediate}$), and slow (τ_{slow}), and their amplitude fractions, that is, fast (A_{fast}), intermediate ($A_{intermediate}$), and slow (A_{slow}), as the kinetic parameters of the recovery from inactivation. As shown in Fig. 5D, TCE at a 3 mM concentration increased the τ_{fast} (126.5 ± 2.4% of that in the control, 2.8 ± 0.1 ms for the control, and 3.6 ± 0.2 ms for 3 mM TCE treatment; $n = 7$, $p < 0.01$), whereas decreased A_{fast} (80.9 ± 2.9% of that in the control,

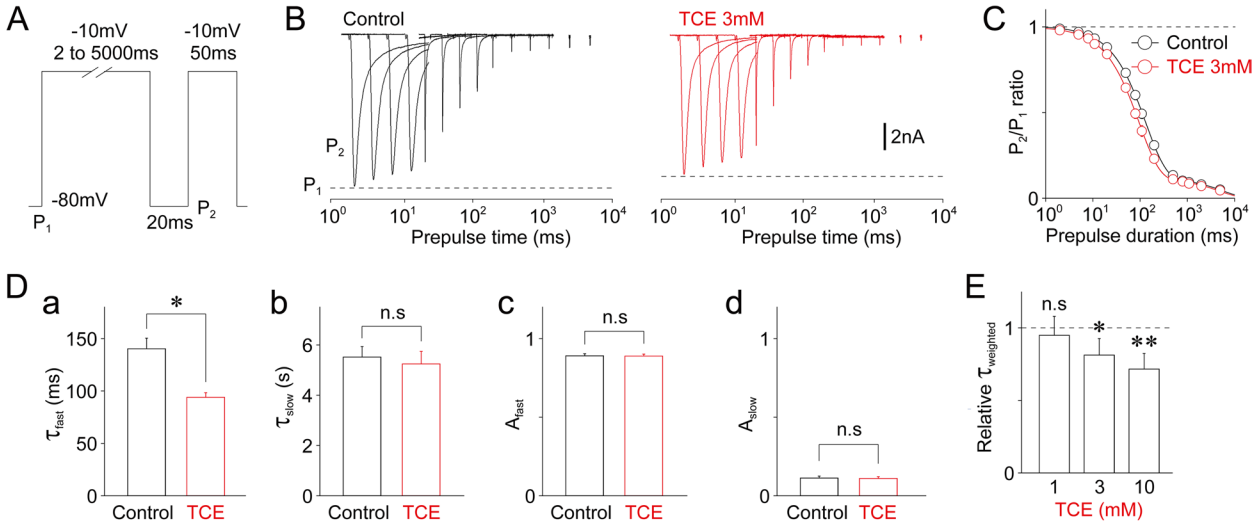

Fig. 4 Effect of TCE on the inactivation of TTX-R Na^+ channels. **(A)** A schematic illustration of the two-pulse protocol for determining inactivation kinetics. The TTX-R I_{Na} was induced by initial conditioning pulses (P_1: − 10 mV depolarization, 2 to 5000 ms duration), which were followed by test pulses (P_2: − 10 mV depolarization, 50 ms duration). The second TTX-R I_{Na} was recovered with an interpulse interval of 20 ms at − 80 mV potential. **(B)** Typical traces of TTX-R I_{Na} elicited by test pulses (P_2) in the two-pulse protocol in the absence (left) and presence (right) of 3 mM TCE. The dotted lines represent the amplitude elicited by the initial conditioning pulses (P_1). **(C)** The P_2/P_1 ratio of TTX-R I_{Na} against the duration of conditioning pulses in the absence (black circles) and presence (red circles) of 3 mM TCE. Continuous lines represent the best fit of the double exponential function. Each point represents the mean and SEM from seven experiments. **(D)** TCE (3 mM)-induced changes in kinetic parameters [**a**: fast time constant (τ_{fast}), **b**: slow time constant (τ_{slow}), **c**: amplitude fraction of fast time constant (A_{fast}), **d**: amplitude fraction of slow time constant (A_{slow}). Each column represents the mean and SEM from seven experiments. **; $p < 0.01$, n.s; not significant. **(E)** TCE (1 mM, 3 mM, and 10 mM)-induced changes in weighted time constant ($\tau_{weighted}$) of the P_2/P_1 ratio of TTX-R I_{Na}. The $\tau_{weighted}$ was normalized to the respective control (dotted line). Each column represents the mean and SEM from seven experiments for 1, 3, and 10 mM TCE. *; $p < 0.05$, **; $p < 0.01$, n.s; not significant

0.47 ± 0.03 for the control and 0.38 ± 0.02 for 3 mM TCE treatment; $n = 7$, $p < 0.01$). However, TCE (3 mM) did not affect the $\tau_{intermediate}$, τ_{slow}, $A_{intermediate}$, and A_{slow} values (Fig. 5D). Notably, TCE increased the $\tau_{weighted}$ in a concentration-dependent manner. In contrast, at a 3 mM concentration, it decreased the $\tau_{weighted}$ (137.0 ± 4.8% of that in the control, 671.1 ± 159.2 ms for the control, and 793.2 ± 156.9 ms for 3 mM TCE treatment; $n = 7$, $p < 0.05$; Fig. 5E).

Effects of TCE on the excitability of small-sized TG neurons

We finally examined whether TCE affected the excitability of small-sized TG neurons under the current-clamp conditions. All current-clamp experiments were performed in the presence of 300 nM TTX. In the presence of TTX, the resting membrane potential of small-sized TG neurons was − 55.9 ± 1.8 mV (− 47.8 to − 62.5 mV, $n = 8$). Moreover, under these conditions, TCE increased the rheobase current, which corresponds to the depolarizing threshold current (T) for the generation of the action potential in a concentration-dependent manner. In contrast, at a 3 mM concentration, it increased the rheobase current to 130.2 ± 5.4% of that in the control (130.0 ± 15.3 pA for the control and 165.7 ± 15.1 pA for 3 mM TCE treatment, $n = 8$, $p < 0.01$, Fig. 6A, Ba, Bb). Notably, TCE also depolarized the membrane potential in a concentration-dependent manner (Fig. 6A, Bc). Small-sized TG neurons were held at a V_H of − 20 mV in a voltage-clamp condition to further examine the mechanism underlying TCE-induced membrane depolarization. TCE induced inwardly directed currents in a concentration-dependent manner (Fig. 6C), and this TCE-induced change in holding current was accompanied by an increase in input resistance (Fig. 6D). Figure 6E shows typical voltage responses elicited by depolarizing current injection [integers of threshold current (1T to 4T)] in the absence and presence of 3 mM TCE. Notably, TCE significantly decreased the number of action potentials elicited by depolarizing current injection in a concentration-dependent manner. In contrast, at a 3 mM concentration, it decreased the number of action potentials elicited by the 4T current injection to 66.5 ± 8.8% of that in the control (6.6 ± 7.5 for the control and 4.4 ± 5.4 for 3 mM TCE treatment, $n = 8$, $p < 0.01$, Fig. 6E, F).

Discussion

Reports on the analgesic efficacy of chloral hydrate remain controversial. While chloral hydrate reportedly exhibits substantial analgesic effects [22], a comprehensive review suggests that chloral hydrate has no analgesic

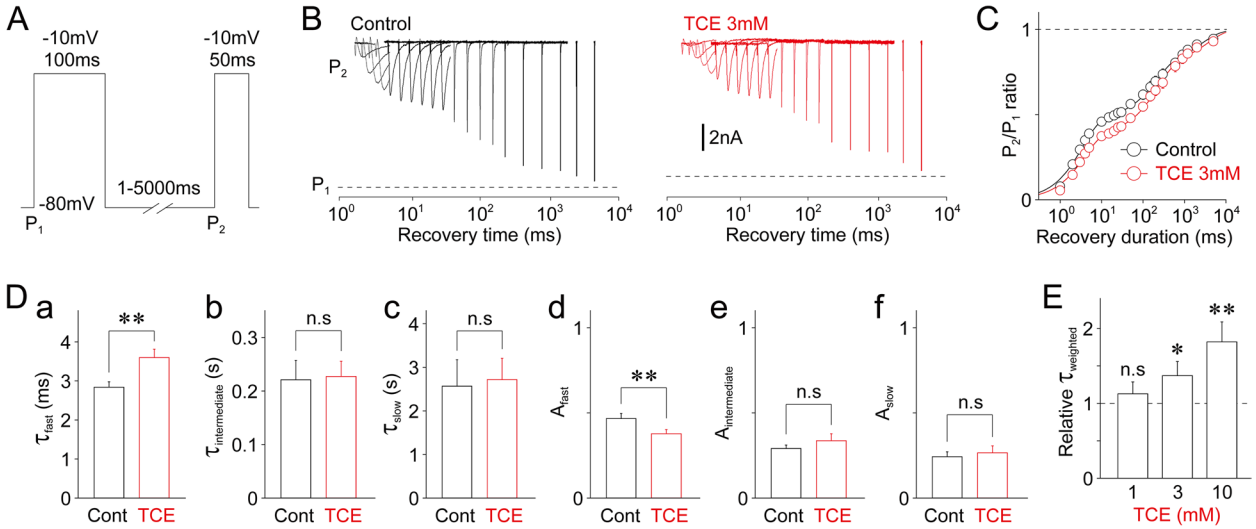

Fig. 5 Effect of TCE on the recovery from inactivation of TTX-R Na^+ channels. **(A)** A schematic illustration of the two-pulse protocol for determining recovery kinetics. The TTX-R I_{Na} was induced by initial conditioning pulses (P_1: − 10 mV depolarization, 100 ms duration), followed by test pulses (P_2: − 10 mV depolarization, 50 ms duration). The second TTX-R I_{Na} was recovered with various interpulse intervals of 1–5000 ms at − 80 mV. **(B)** Typical traces of TTX-R I_{Na} elicited by test pulses (P_2) in the two-pulse protocol in the absence (left) and presence (right) of 3 mM TCE. The dotted lines represent the amplitude elicited by conditioning pulses (P_1). **(C)** The P_2/P_1 ratio of TTX-R I_{Na} against the duration of conditioning pulses in the absence (black circles) and presence (red circles) of 3 mM TCE. Continuous lines represent the best fit of the double exponential function. Each point represents the mean and SEM from seven experiments. **(D)** TCE (3 mM)-induced changes in kinetic parameters [**a**: fast time constant (τ_{fast}), **b**: intermediate time constant ($\tau_{intermediate}$), **c**: slow time constant (τ_{slow}), **d**: amplitude fraction of fast time constant (A_{fast}), amplitude fraction of intermediate time constant ($A_{intermediate}$), **f**: amplitude fraction of slow time constant (A_{slow}). Each column represents the mean and SEM from seven experiments. **; $p < 0.01$, n.s; not significant. **(E)** TCE (1, 3, and 10 mM)-induced changes in weighted time constant ($\tau_{weighted}$) of the P_2/P_1 ratio of TTX-R I_{Na}. The $\tau_{weighted}$ was normalized to the respective control (dotted line). Each column represents the mean and SEM from seven experiments for 1, 3, and 10 mM TCE. *; $p < 0.05$, **; $p < 0.01$, n.s; not significant

properties [7]. Several lines of evidence have suggested that chloral hydrate, through its active metabolite TCE, acts on both the central and peripheral nervous system to elicit analgesic effects. For example, TCE-induced potentiation of central $GABA_A$ receptors might contribute to the analgesic effects mediated by chloral hydrate [15, 16], as benzodiazepines, which also potentiate central $GABA_A$ receptors, have long been considered primary or adjunctive analgesics [26]. TCE reportedly inhibits P2 × 3 receptors and, to a limited extent, P2Y receptors in nociceptive neurons of the DRG [20], suggesting that TCE-induced inhibition of P2 receptors might contribute to its peripheral analgesic effects. Furthermore, TCE activates non-classical two-pore-domain K^+ (K2P) channels, including recombinant or native TREK-1 (KCNK2) and TRAAK (KCNK4) [27–29] at clinically relevant concentrations. Given that these K2P subtypes are also expressed in nociceptive sensory neurons [30, 31] and that the activation of K2P channels, such as TREK-1, is partly responsible for the analgesic efficacy of volatile anesthetics [32, 33], we speculated that K2P channels might be involved in mediating the chloral hydrate-induced analgesic effects.

Our present study provided additional evidence that TCE acts peripherally to exert analgesic effects by inhibiting or modulating TTX-R Na^+ channels, as these channels play pivotal roles in action potential electrogenesis in nociceptive sensory neurons [3]. We observed that TCE decreased the peak amplitude of TTX-R I_{Na} in a concentration-dependent manner with an IC_{50} value of 18 mM. Considering that the peak plasma concentration of TCE reaches low millimolar concentrations (2–5 mM) after orally administering high doses (> 2.0 g) of chloral hydrate ([14, 34], but see also [13]), TCE at clinically relevant concentrations could elicit small but significant inhibition of TTX-R Na^+ channels expressed in nociceptive neurons. We also demonstrated that TCE decreased the decay time constant of single TTX-R I_{Na} in a concentration-dependent manner, suggesting that TCE accelerates the deactivation of TTX-R Na^+ channels. Collectively, these results suggest that chloral hydrate, through its active metabolite TCE, directly acts on peripheral Na^+ channels to decrease nociceptive transmission. In this context, examining whether TCE has direct inhibitory effects on $Na_V1.7$ and $Na_V1.9$, TTX-S and TTX-R Na^+ channel subtypes, expressed in nociceptive sensory neurons bears significance [1].

Notably, I_{NaP} mediated by voltage-gated Na^+ channels has been implicated in the firing patterns of neurons,

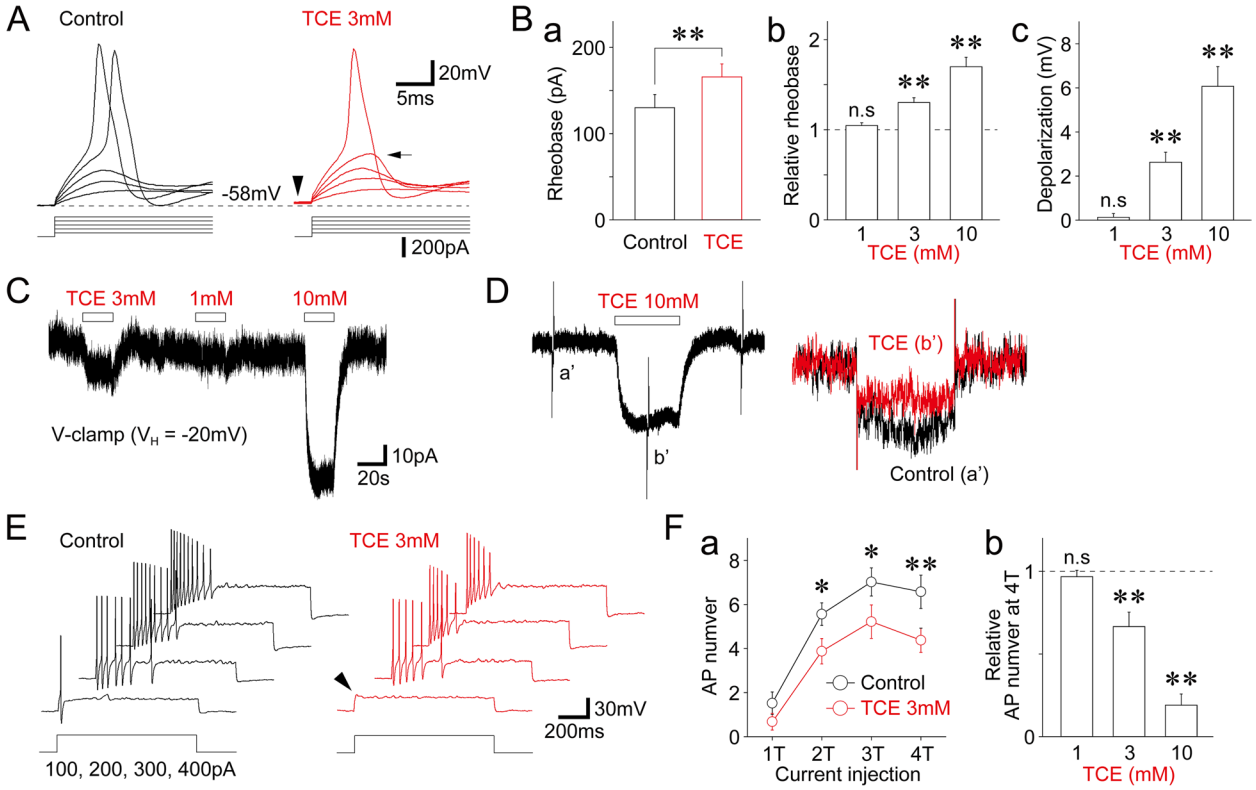

Fig. 6 Effect of TCE on the excitability of small-sized TG neurons. **(A)** Typical voltage traces in response to depolarizing current injection in the absence (left) and presence (right) of 3 mM TCE. Five representative raw traces were elicited by successive depolarizing current injection (40–200 pA, 40 pA increment). Note that action potential was not triggered by the fourth stimulation (160 pA injection, arrow), whereas the membrane potential was depolarized (arrowhead) in the presence of 3 mM TCE. **(B) a**, TCE (3 mM)-induced changes in the absolute amplitude of rheobase currents. Each column represents the mean and SEM from eight experiments. **; $p < 0.01$. **b**, TCE (1, 3, and 10 mM)-induced changes in the amplitude of rheobase currents. Each column was normalized to the respective control (dotted line) and represents the mean and SEM from seven, eight, and eight experiments for 1, 3, and 10 mM TCE, respectively. **; $p < 0.01$, n.s; not significant. **c**, TCE (1, 3, and 10 mM)-induced changes in membrane potential. Each column represents the mean and SEM from seven, eight, and eight experiments for 1, 3, and 10 mM TCE, respectively. **; $p < 0.01$, n.s; not significant. **(C)** A typical current trace before, during, and after applying various concentrations of TCE. Small-sized TG neurons were held at a V_H of − 20 mM in a voltage-clamp (V-clamp) condition. **(D)** A typical current trace in response to 10-mV hyperpolarizing voltage steps (300-ms duration) before, during, and after applying 10 mM TCE at a V_H of − 20 mV. Inset (right) represents typical current traces (a′ and b′) with an expanded time scale. **(E)** Typical voltage traces in response to depolarizing current injection before (left) and during (right) the application of 3 mM TCE. Four representative raw traces were elicited by a one-fold threshold (1T; 100 pA) to the four-fold threshold (4T; 400 pA) depolarizing current injection. Note that the 1T stimulation did not trigger action potentials in the presence of 3 mM TCE (arrowhead). **(F) a**, Changes in the number of action potentials elicited by depolarizing current injection (1T to 4T) in the absence (black circles) and presence (red circles) of 3 mM TCE. Each point represents the mean and SEM from eight experiments. **b**, TCE (1, 3, and 10 mM)-induced changes in the number of action potentials elicited by 4T-depolarizing current injection. Each column was normalized to the respective control (dotted line) and represents the mean and SEM from seven, eight, and eight experiments for 1, 3, and 10 mM TCE, respectively. **; $p < 0.01$, n.s; not significant

such as regular and repetitive firing, in various regions of the brain [35–38]. Furthermore, I_{NaP} is involved in regulating neuronal excitability, including resting membrane potentials, spike initiation, and burst generation of action potentials [39–42]. Moreover, I_{NaP} mediated by TTX-R Na^+ channels reportedly contributes to the firing frequency of nociceptive sensory neurons [5, 43]. Furthermore, an abnormal increase in I_{NaP} has been implicated in neurological disorders, such as epilepsy and pain, with excessive neuronal excitability [44–46]. When transfected in $Na_V1.8$-knockout mouse DRG neurons, human $Na_V1.8$ exhibits larger TTX-R I_{NaP} and I_{Ramp} than rat $Na_V1.8$ [43]. Furthermore, $Na_V1.8$-mediated I_{NaP} along with the firing frequency in response to depolarizing current stimuli are significantly higher in human DRG neurons than in rat DRG neurons [43]. Since the density of TTX-R I_{NaP} or I_{Ramp} is closely related to the firing frequency of nociceptive neurons [5], the pharmacological manipulation of TTX-R I_{NaP} would be a new strategy for the treatment of various pain conditions. In the present study, TCE potently inhibited the TTX-R I_{NaP} and I_{Ramp} with

an IC_{50} values of 3.3 mM and 2.0 mM, respectively, and that TCE, even at submillimolar concentrations, slightly but significantly inhibited the non-inactivating currents mediated by TTX-R Na^+ channels. Therefore, we inferred that the preferential inhibition of TTX-R I_{NaP} by TCE would be responsible for the analgesic efficacy of chloral hydrate.

In addition to the direct inhibition of transient TTX-R I_{Na} and I_{NaP}, TCE had multiple effects on various properties of TTX-R Na^+ channels. First, TCE shifted the voltage-activation and -inactivation relationships toward hyperpolarizing potentials. As voltage dependence is the fundamental property that determines channel activation and inactivation according to the change in membrane potentials [47], TTX-R Na^+ channels might be further inactivated at resting membrane potentials in the presence of TCE. Second, TCE accelerated the extent of the onset of TTX-R Na^+ channel inactivation in a concentration-dependent manner. Specifically, TCE decreased τ_{fast} rather than τ_{slow}, consistent with an acceleration of the fast rather than slow components of TTX-R Na^+ channel inactivation. Third, TCE retarded the recovery from the inactivation of TTX-R Na^+ channels in a concentration-dependent manner. In contrast, it increased τ_{fast} rather than τ_{slow}, consistent with the retardation of the fast component of recovery kinetics of TTX-R Na^+ channels. Finally, TCE increased the extent of use-dependent inhibition of TTX-R Na^+ channels. As the use-dependent inhibition, as well as the inactivation and recovery kinetics, are directly related to the repetitive generation of action potentials at higher frequencies, TCE might contribute to the inhibition of repetitive action potential generation during sustained depolarization.

Previous studies using a combination of site-specific mutagenesis and patch-clamp technique have revealed the concrete binding sites of TCE to several ion channels. For example, in the $GABA_A$ receptors containing α2 and β1 subunits, a specific mutation within transmembrane domain 3 of the β1 subunit (M286W) abolishes TCE-induced potentiation of Cl^- current [16]. In contrast, low concentrations of TCE do not enhance the Cl^- current mediated by glycine receptors with two specific mutations α1 subunit (S267I and A288W) [16]. The TCE sensitivity to NMDA receptors is also altered by specific mutations in the GluN2A subunit (F637W and A825W) [48]. Finally, the positive modulation of 5-HT3A receptors by TCE is dramatically reduced by the R246A mutation [49]. At this stage, however, the mechanism by which TCE inhibits and modulates various properties of TTX-R Na^+ channels remains unknown. As TCE is a lipophilic compound with an octanol/buffer partition coefficient of 1.42, it is expected to incorporate hydrophobic compartments, such as lipid membrane, with the subsequent hydrophobic interactions with channel proteins being potentially responsible for the modulation of TTX-R Na^+ channels. A simulation study suggested that TCE could bind to protein targets with higher affinities, suggesting that it might bind to ion channels during membrane partition [50]. This molecular behavior is similar to that of volatile anesthetics, such as isoflurane and sevoflurane, which exhibit a distinct preference for the membrane interface [51]. However, the possibility that TCE directly interacts with the outer vestibule of TTX-R Na^+ channels cannot be excluded. Considering that lysine 806 in domain II of $Na_V1.8$ plays a role in the high sensitivity of $Na_V1.8$ to open-channel blockage by *n*-alcohol [52], a combination of site-specific mutagenesis and patch-clamp technique may reveal the detailed binding sites and mechanisms underlying TCE-mediated modulation of TTX-R Na^+ channels.

In the present study, TCE increased the amplitude of rheobase current to generate action potentials but decreased the number of action potentials elicited by depolarizing current stimuli. Considering that I_{NaP} plays crucial roles in the repetitive generation of action potentials in central neurons within various brain regions [38–42, 53] and that TTX-R I_{NaP} contributes to the excitability of nociceptive sensory neurons [5], we speculated that the preferential inhibition of TTX-R I_{NaP} mediates TCE-induced changes in the number of action potentials. The modulation of inactivation and recovery kinetics and use-dependent inhibition of TTX-R Na^+ channels might be additionally responsible for the TCE-induced changes in neuronal excitability. We previously reported that TTX-R I_{NaP} is closely related to the inactivation and recovery kinetics and use-dependent inhibition of TTX-R Na^+ channels in nociceptive sensory neurons [5]. Furthermore, we also observed that TCE slightly depolarized the membrane potential. This TCE-induced membrane depolarization might be mediated by the inhibition of leak K^+ channels, such as K2P channels because the TCE-induced decrease in holding current was accompanied by an increase in input resistance. However, as TCE at a higher concentration (10 mM) exhibited significant changes in input resistance, the effect of TCE at a clinically relevant concentration on input resistance would be negligible.

Conclusion

In conclusion, we demonstrated that TCE, an active metabolite of chloral hydrate, inhibited the TTX-R I_{Na} and modulated various properties of these channels at clinically relevant concentrations, resulting in decreased excitability of nociceptive neurons. These pharmacological characteristics provide novel evidence for the analgesic efficacy mediated by chloral hydrate in pediatric dentistry.

Abbreviations

DRG	dorsalroot ganglia
I_{Na}	Na^+current
I_{NaP}	persistentI_{Na}
I_{NaT}	transient I_{Na}
I_{Ramp}	slow voltage-ramp-induced current
TCE	2′,2′,2′-trichloroethanol
TG	trigeminalganglia
TTX-R	tetrodotoxin-resistant
TTX-S	tetrodotoxin-sensitive

Acknowledgements
We would like to thank Editage (www.editage.co.kr) for English language editing.

Authors' contributions
G.K., H.K., and I.-S.J. designed the study. G.K. and I.-S.J. performed the experiments. G.K. and I.-S.J. wrote the manuscript. I.-S.J. made further critical manuscript revisions. G.K., H.K., and I.-S.J. read and approved the final manuscript.

Funding
This work was supported by the National Research Foundation of Korea (NRF) grant funded by the Korea government (MSIP) (2021R1A2C1011583).

Availability of data and materials
The datasets used and/or analysed during the current study are available from the corresponding author on reasonable request.

Declarations

Ethics approval and consent to participate
All experiments were conducted in accordance with approved animal protocols and guidelines established by the Animal Care Committee of Kyungpook National University (Approval No. KNU-2019-0053). Animal studies are reported in compliance with the ARRIVE guidelines, and every effort was made to minimize both the number of animals used and their suffering.

Consent for publication
Not applicable.

Competing interests
The authors declare no competing interests.

Author details
[1]Department of Pediatric Dentistry, School of Dentistry, Kyungpook National University, Daegu 41940, Republic of Korea. [2]Department of Pharmacology, School of Dentistry, Kyungpook National University, 2177 Dalgubeol-daero, Jung-gu, Daegu 41940, Republic of Korea. [3]Brain Science & Engineering Institute, Kyungpook National University, Daegu 41940, Republic of Korea.

Received: 22 December 2022 Accepted: 22 April 2023
Published online: 29 April 2023

References

1. Dib-Hajj SD, Waxman SG. Sodium channels in Human Pain Disorders: Genetics and Pharmacogenomics. Annu Rev Neurosci. 2019;42:87–106.
2. England S, Bevan S, Docherty RJ. PGE_2 modulates the tetrodotoxin-resistant sodium current in neonatal rat dorsal root ganglion neurones via the cyclic AMP-protein kinase a cascade. J Physiol. 1996;495:429–40.
3. Renganathan M, Cummins TR, Waxman SG. Contribution of $Na_V1.8$ sodium channels to action potential electrogenesis in DRG neurons. J Neurophysiol. 2001;86:629–40.
4. Gold MS, Gebhart GF. Nociceptor sensitization in pain pathogenesis. Nat Med. 2010;16:1248–57.
5. Nakamura M, Jang IS. Contribution of tetrodotoxin-resistant persistent Na^+ currents to the excitability of C-type dural afferent neurons in rats. J Headache Pain. 2022;23:73.
6. Tobias JD. Sedation and analgesia in paediatric intensive care units: a guide to drug selection and use. Paediatr Drugs. 1999;1:109–26.
7. Krauss B, Green SM. Procedural sedation and analgesia in children. Lancet. 2006;367:766–80.
8. Pershad J, Palmisano P, Nichols M. Chloral hydrate: the good and the bad. Pediatr Emerg Care. 1999;15:432–5.
9. Tobias JD. Applications of nitrous oxide for procedural sedation in the pediatric population. Pediatr Emerg Care. 2013;29:245–65.
10. Silverman J, Muir. WW 3rd. A review of laboratory animal anesthesia with chloral hydrate and chloralose. Lab Anim Sci. 1993;43:210–6.
11. Cabana BE, Gessner PK. The kinetics of chloral hydrate metabolism in mice and the effect thereon of ethanol. J Pharmacol Exp Ther. 1970;174:260–75.
12. Gessner PK, Cabana BE. A study of the interaction of the hypnotic effects and of the toxic effects of chloral hydrate and ethanol. J Pharmacol Exp Ther. 1970;174:247–59.
13. Merdink JL, Robison LM, Stevens DK, Hu M, Parker JC, Bull RJ. Kinetics of chloral hydrate and its metabolites in male human volunteers. Toxicology. 2008;245:130–40.
14. Breimer DD. Clinical pharmacokinetics of hypnotics. Clin Pharmacokinet. 1977;2:93–109.
15. Peoples RW, Weight FF. Trichloroethanol potentiation of gamma-aminobutyric acid-activated chloride current in mouse hippocampal neurones. Br J Pharmacol. 1994;113:555–63.
16. Krasowski MD, Finn SE, Ye Q, Harrison NL. Trichloroethanol modulation of recombinant $GABA_A$, glycine and GABA rho 1 receptors. J Pharmacol Exp Ther. 1998;284:934–42.
17. Pistis M, Belelli D, Peters JA, Lambert JJ. The interaction of general anaesthetics with recombinant $GABA_A$ and glycine receptors expressed in Xenopus laevis oocytes: a comparative study. Br J Pharmacol. 1997;122:1707–19.
18. Downie DL, Hope AG, Belelli D, Lambert JJ, Peters JA, Bentley KR, Steward LJ, Chen CY, Barnes NM. The interaction of trichloroethanol with murine recombinant 5-HT_3 receptors. Br J Pharmacol. 1995;114:1641–51.
19. Scheibler P, Kronfeld A, Illes P, Allgaier C. Trichloroethanol impairs NMDA receptor function in rat mesencephalic and cortical neurones. Eur J Pharmacol. 1999;366:R1–R2.
20. Fischer W, Wirkner K, Weber M, Eberts C, Köles L, Reinhardt R, et al. Characterization of P2X3, P2Y1 and P2Y4 receptors in cultured HEK293-hP2X3 cells and their inhibition by ethanol and trichloroethanol. J Neurochem. 2003;85:779–90.
21. Zaugg M, Lucchinetti E, Spahn DR, Pasch T, Garcia C, Schaub MC. Differential effects of anesthetics on mitochondrial K_{ATP} channel activity and cardiomyocyte protection. Anesthesiology. 2002l;97:15–23.
22. Field KJ, White WJ, Lang CM. Anaesthetic effects of chloral hydrate, pentobarbitone and urethane in adult male rats. Lab Anim. 1993;27:258–69.
23. Murase K, Ryu PD, Randic M. Excitatory and inhibitory amino acids and peptide-induced responses in acutely isolated rat spinal dorsal horn neurons. Neurosci Lett. 1989;103:56–63.
24. Fleidervish IA, Gutnick MJ. Kinetics of slow inactivation of persistent sodium current in layer V neurons of mouse neocortical slices. J Neurophysiol. 1996;76:2125–30.
25. Magistretti J, Alonso A. Biophysical properties and slow voltage-dependent inactivation of a sustained sodium current in entorhinal cortex layer-II principal neurons: a whole-cell and single-channel study. J Gen Physiol. 1999;114:491–509.
26. Wright SL. Limited utility for Benzodiazepines in Chronic Pain Management: a narrative review. Adv Ther. 2020;37:2604–19.
27. Harinath S, Sikdar SK. Trichloroethanol enhances the activity of recombinant human TREK-1 and TRAAK channels. Neuropharmacology. 2004;46:750–60.
28. Bryan RM Jr, You J, Phillips SC, Andresen JJ, Lloyd EE, Rogers PA, et al. Evidence for two-pore domain potassium channels in rat cerebral arteries. Am J Physiol Heart Circ Physiol. 2006;291:H770–80.
29. Parelkar NK, Silswal N, Jansen K, Vaughn J, Bryan RM Jr, Andresen J. 2,2,2-trichloroethanol activates a nonclassical potassium channel in cerebrovascular smooth muscle and dilates the middle cerebral artery. J Pharmacol Exp Ther. 2010;332:803–10.

30. Smith PA. K^+ channels in primary afferents and their role in nerve Injury-Induced Pain. Front Cell Neurosci. 2020;14:566418.
31. Gada K, Plant LD. Two-pore domain potassium channels: emerging targets for novel analgesic drugs: IUPHAR Review 26. Br J Pharmacol. 2019;176:256–66.
32. Tong L, Cai M, Huang Y, Zhang H, Su B, Li Z, et al. Activation of K_2P channel-TREK1 mediates the neuroprotection induced by sevoflurane preconditioning. Br J Anaesth. 2014;113:157–67.
33. Franks NP, Lieb WR. Background K^+ channels: an important target for volatile anesthetics? Nat Neurosci. 1999;2:395–6.
34. Owen BE, Taberner PV. Studies on the hypnotic effects of chloral hydrate and ethanol and their metabolism in vivo and in vitro. Biochem Pharmacol. 1980;29:3011–6.
35. Taddese A, Bean BP. Subthreshold sodium current from rapidly inactivating sodium channels drives spontaneous firing of tuberomammillary neurons. Neuron. 2002;33:587–600.
36. Bennett BD, Callaway JC, Wilson CJ. Intrinsic membrane properties underlying spontaneous tonic firing in neostriatal cholinergic interneurons. J Neurosci. 2000;20:8493–503.
37. Zeng J, Powers RK, Newkirk G, Yonkers M, Binder MD. Contribution of persistent sodium currents to spike-frequency adaptation in rat hypoglossal motoneurons. J Neurophysiol. 2005;93:1035–41.
38. Cho JH, Choi IS, Lee SH, Lee MG, Jang IS. Contribution of persistent sodium currents to the excitability of tonic firing substantia gelatinosa neurons of the rat. Neurosci Lett. 2015;591:192–6.
39. Wu N, Enomoto A, Tanaka S, Hsiao CF, Nykamp DQ, Izhikevich E, et al. Persistent sodium currents in mesencephalic V neurons participate in burst generation and control of membrane excitability. J Neurophysiol. 2005;93:2710–22.
40. Enomoto A, Han JM, Hsiao CF, Wu N, Chandler SH. Participation of sodium currents in burst generation and control of membrane excitability in mesencephalic trigeminal neurons. J Neurosci. 2006;26:3412–22.
41. Kuo JJ, Lee RH, Zhang L, Heckman CJ. Essential role of the persistent sodium current in spike initiation during slowly rising inputs in mouse spinal neurones. J Physiol. 2006;574:819–34.
42. Lamas JA, Romero M, Reboreda A, Sanchez E, Ribeiro SJ. A riluzole- and valproate-sensitive persistent sodium current contributes to the resting membrane potential and increases the excitability of sympathetic neurones. Pflügers Arch. 2009;458:589–99.
43. Han C, Estacion M, Huang J, Vasylyev D, Zhao P, Dib-Hajj SD, et al. Human $Na_V1.8$: enhanced persistent and ramp currents contribute to distinct firing properties of human DRG neurons. J Neurophysiol. 2015;113:3172–85.
44. Meisler MH, Kearney JA. Sodium channel mutations in epilepsy and other neurological disorders. J Clin Invest. 2005;115:2010–7.
45. Stafstrom CE. Persistent sodium current and its role in epilepsy. Epilepsy Curr. 2007;7:15–22.
46. Mantegazza M, Curia G, Biagini G, Ragsdale DS, Avoli M. Voltage-gated sodium channels as therapeutic targets in epilepsy and other neurological disorders. Lancet Neurol. 2010;9:413–24.
47. Wisedchaisri G, Gamal El-Din TM. Druggability of Voltage-Gated Sodium channels-exploring old and new drug receptor Sites. Front Pharmacol. 2022;13:858348.
48. Salous AK, Ren H, Lamb KA, Hu XQ, Lipsky RH, Peoples RW. Differential actions of ethanol and trichloroethanol at sites in the M3 and M4 domains of the NMDA receptor GluN2A (NR2A) subunit. Br J Pharmacol. 2009;158:1395–404.
49. Hu XQ, Peoples RW. Arginine 246 of the pretransmembrane domain 1 region alters 2,2,2-trichloroethanol action in the 5-hydroxytryptamine3A receptor. J Pharmacol Exp Ther. 2008;324:1011–8.
50. Kiametis AS, Stock L, Cirqueira L, Treptow W. Atomistic model for simulations of the Sedative Hypnotic Drug 2,2,2-Trichloroethanol. ACS Omega. 2018;3:15916–23.
51. Arcario MJ, Mayne CG, Tajkhorshid E. Atomistic models of general anesthetics for use in in silico biological studies. J Phys Chem B. 2014;118:12075–86.
52. Horishita T, Harris RA. *n*-Alcohols inhibit voltage-gated Na^+ channels expressed in *Xenopus* oocytes. J Pharmacol Exp Ther. 2008;326:270–7.
53. Cummins TR, Howe JR, Waxman SG. Slow closed-state inactivation: a novel mechanism underlying ramp currents in cells expressing the hNE/PN1 sodium channel. J Neurosci. 1998;18:9607–19.

Publisher's Note